

Analyst

Accepted Manuscript



This is an *Accepted Manuscript*, which has been through the Royal Society of Chemistry peer review process and has been accepted for publication.

Accepted Manuscripts are published online shortly after acceptance, before technical editing, formatting and proof reading. Using this free service, authors can make their results available to the community, in citable form, before we publish the edited article. We will replace this *Accepted Manuscript* with the edited and formatted *Advance Article* as soon as it is available.

You can find more information about *Accepted Manuscripts* in the [Information for Authors](#).

Please note that technical editing may introduce minor changes to the text and/or graphics, which may alter content. The journal's standard [Terms & Conditions](#) and the [Ethical guidelines](#) still apply. In no event shall the Royal Society of Chemistry be held responsible for any errors or omissions in this *Accepted Manuscript* or any consequences arising from the use of any information it contains.

A novel Zinc(II) and Hydrogen sulphate selective fluorescent "turn-on" chemosensor based on isonicotiamide: INHIBIT type's logic gate and application in cancer cell imaging

Kundan Tayade^{*a}, Banashree Bondhopadhyay^e, Karunesh Keshav^c, Suban K. Sahoo^b, Anupam Basu^e, Jasmider Singh^d, Narinder Singh^d, Dileep T.Nehete^f, Anil Kuwar^{*a}

^aSchool of Chemical Sciences, North Maharashtra University, Jalgaon-425001 (MS), India.

^bDepartment of Applied Chemistry, SV National Institute of Technology, Surat-395007 (Gujrat), India.

^cDepartment of Chemistry, Indian Institute of Science Education and Research, Bhopal- 462 066 (Madhya Pradesh) India.

^dDepartment of Chemistry, Indian Institute of Technology, Ropar, Rupnagar (Punjab), India.

^eMolecular Biology and Human Genetics Laboratory, Department of Zoology, The University of Burdwan, Burdwan, West Bengal, India.

^fDepartment of Chemistry, M.J College, Jalgaon-425001 (MS), India.

Abstract

We have developed a novel isonicotiamide-based fluorescent "turn-on" Chemosensor **1** for the selective detection of Zn^{2+} and HSO_4^- . The sensor **1** can detect Zn^{2+} and HSO_4^- with the detection limit down to nanomolar level by forming a complex in 1:1 stoichiometry in the presence of other anions and 2:1 in presence of cations in aqueous solution. Density functional theory calculations on **1** and the **1**- $\text{Zn}^{2+}/\text{HSO}_4^-$ complexes are consistent with the experimental results. We have successfully utilized the above cation and anion for the fabrication of INHIBIT molecular logic gates. Furthermore the receptor **1** was successfully detect the Zn^{2+} and HSO_4^- ions in HeLa cells cultured in Zn^{2+} and HSO_4^- enriched medium.

***Corresponding authors:** E-mail: kuwaras@gmail.com, kundantayade@gmail.com

Tel.:+91-257-2257432; Fax: +91-257-2257403.

1. Introduction

The design of synthetic chemosensors for the discovery and selective sensing of cations and anions has gained immense interest from the last few decades because of their significant tasks and prospective functions in the field of material, environmental and biological sciences [1-5]. Among the various transition metal ions, numerous scientific endeavours have been focused for the development of novel chemo-sensing systems for the zinc ion due to its biological significance [6-9]. After iron, zinc is the second most abundant transition metal ion in the human body and known to play vital functions in many biological functions including brain movement, gene transcription and neural signal transmitters or modulators. As zinc acts as a structural cofactor in many enzymatic processes, the deficiency of zinc causes unbalanced metabolism and progression of many disorders such as Alzheimer's disease, epilepsy, Parkinson's disease, ischemic stroke and infantile diarrhoea. Similarly, the anion HSO_4^- has a number of biological functions and known to produce toxic sulfate (SO_4^{2-}) ions at alkaline high pH, causing diseases relating to skin, eyes and respiratory system [10-12]. Therefore, the sensing of Zn^{2+} and HSO_4^- has drawn growing curiosity in the chemical and biological sciences. However, it is very challenging to develop suitable chemo-sensing systems for the selective detection of Zn^{2+} and HSO_4^- . Zinc (II) is spectroscopically and magnetically silent due to the fully filled ($3d^{10} 4s^0$) electronic configuration. Additionally, the sensing of Zn^{2+} is interfered in the presence of Cd^{2+} because of the similar coordinating properties and spectral changes, as both are placed in the same group of the periodic table. Similarly, anion recognition is challenging due to their large size (lower charge to radius ratio), different basicity, highly sensitive to pH and different geometries such as spherical, linear, trigonal, tetrahedral and octahedral.

In the middle of the variety of chemo-sensing systems expanded up to now for the detection of cations and anions, the fluorogenic sensor has attracted a great deal of choice due

1
2
3 to the simplicity, sky-scraping sensitivity and selectivity [13-15]. To the best of our
4
5 knowledge, the isonicotiamide based sensors reported so far are based on fluorescence
6
7 quenching process for a specific cation or anion. The isonicotiamide based sensors that are
8
9 capable for detecting multiple cations and anions by fluorescence enhancement process are
10
11 very rare. Here, the functioning of sensor **1** for recognizing Zn^{2+} and HSO_4^- is based on the
12
13 appended isonicotiamide functionalities that act as a binding as well as a fluorescent 'turn-on'
14
15 sensing unit by inhibiting the C=N isomerisation at the excited state. The recognition process
16
17 has been recommended to involve the coordination and hydrogen bonding interactions of the
18
19 Zn^{2+} and HSO_4^- ions with the Chemosensor **1**.

22 23 **Scheme 1.**

24 25 **2. Experimental**

26 27 **2.1. Materials and methods**

28
29 All reagents and chemicals were purchased from Aldrich Chemicals Ltd and were
30
31 used without further purification. The solvents were distilled before used. All reactions were
32
33 magnetically stirred and monitored by thin-layer chromatography (TLC). ^1H and ^{13}C NMR
34
35 spectra were obtained on a Bruker AVANCE DMX400 spectrometer in DMSO-d_6 as solvent.
36
37 Fluorescence measurements were made with a HORIBA JOBIN YVON, Fluoromax-4
38
39 Spectrofluorometer equipped with a xenon lamp. UV-Vis absorption spectra were recorded
40
41 on a Shimadzu UV-2450 spectrophotometer.
42
43
44

45 46 **2.2. Synthesis of Chemosensor 1**

47
48 The solution of 3.5 mg isonicotinohydrazide (1 mmol) in ethanol (25 mL) was added
49
50 to a solution of 3 mg of 2-amino pyridine-3-carbaldehyde (1 mmol) in ethanol (25 mL) at
51
52 room temperature. Then, the reaction mixture was stirred and refluxed for 6 hrs. The reaction
53
54 mixture was cooled and the precipitate was filtered followed by washed with cold ethanol and
55
56 dried under vacuum (yield: 85 %). ^1H NMR (400 MHz, DMSO-d_6): $\delta = 4.12$ (s, 2H, NH_2),
57
58
59
60

1
2
3 6.79(t, 1H, 9 Hz Py-H), 7.10 (s, 1H, NH), 7.67 (s, 1H, CH=N), 8.09 (d, 8 Hz, 2H, Py-H), 8.15
4
5 (d, 1H, 8 Hz Py-H), 8.50 (d, 1H, 8 Hz, Py-H), 9.12 (d, 2H, 8 Hz Py-H) ppm. ^{13}C NMR (100
6
7 MHz, DMSO- d_6): δ = 111.6, 113.5, 123.0, 139.1, 141.2, 143.1, 150.3, 151.3, 165.1 ppm.

10 2.3. X-ray crystal structure determination

11
12 Diffraction quality crystal of the Chemosensor **1** was obtained by slow evaporation of
13
14 a reaction mixture solution. X-ray diffraction data for the crystals mounted on a glass fibre
15
16 and coated with perfluoropolyether oil were collected on a Bruker-AXS SMART APEX II
17
18 diffractometer at room temperature equipped with CCD detector using graphite-
19
20 monochromatic Mo-K α radiation ($\lambda = 0.71073 \text{ \AA}$). The data were processed with SAINT and
21
22 absorption corrections were made with SADABS. The structure was solved by direct and
23
24 Fourier methods and refined by full-matrix least-square based on F^2 using the WINGX
25
26 software which utilizes SHELX-97 [16]. For structure solution and refinement the SHELXTL
27
28 software package was used. The non-hydrogen atoms were refined anisotropically, while the
29
30 hydrogen atoms were placed with fixed thermal parameters at idealized positions.
31
32

34 2.4. UV–Visible and fluorescence spectral measurements

35
36 For UV–Vis and fluorescence spectroscopy, the metal ions Na^+ , K^+ , Ca^{2+} , Mg^{2+} , Al^{3+} ,
37
38 Fe^{2+} , Fe^{3+} , Co^{2+} , Ni^{2+} , Cu^{2+} , Zn^{2+} (100 μM) were added as their nitrates, Sr^{2+} , Cr^{3+} , Mn^{2+}
39
40 were added as their chlorides, Ba^{2+} , Cs^+ , Bi^{3+} , Cd^{2+} , Hg^{2+} , Pb^{2+} , Th^{4+} , Ag^+ were added as their
41
42 nitrates, Zr^{4+} was added as its oxychloride while U^{6+} was added as its sulphate. The tetrabutyl
43
44 ammonium salts of anions such as F^- , I^- , Cl^- , CN^- , NO_3^- , Br^- , and HSO_4^- (100 μM) were
45
46 used, along with sodium salts of various oxyanions of sulphur (SO_3^- , HSO_3^- and S_2O_5^-). The
47
48 solutions of cations and anions were prepared in 50 % aqueous CH_3CN containing ($c = 100$
49
50 μM) for analysis with Chemosensor **1**. The solution of Chemosensor **1** was freshly prepared
51
52 in 50 % aqueous CH_3CN ($c = 10 \mu\text{M}$). The excitation was carried out at 300 nm for
53
54
55
56
57
58
59
60

1
2
3 Chemosensor **1** with 3 nm emission slit widths in fluorimeter. For absorbance and
4
5 fluorescence measurements 1 cm width and 3.5 cm height quartz cells were used.
6

7
8 The binding stoichiometry of **1** with Zn^{2+} and HSO_4^- were determined by using a
9
10 Job's plot. For the Job's plot analyses, a series of solutions with varying mole fractions of the
11
12 cations and anions were prepared by maintaining the total concentration of **1** and Zn^{2+} and
13
14 HSO_4^- constant. The fluorescence emission was measured for each sample by exciting it at
15
16 300 nm and the spectra were measured from 320 to 620 nm. The maximum fluorescence
17
18 intensity at 470 nm and 425 nm for each solution was plotted against the mole fraction of the
19
20 Zn^{2+} and HSO_4^- ion respectively.
21
22

23 **2.5 In vitro cell imaging**

24
25 HeLa cells were procured from National Centre for Cell Sciences, Pune, India and
26
27 grown in Dulbecco's Modified Eagle Medium (DMEM) supplemented with 10% Fetal
28
29 Bovine Serum (FBS), 1% L-glutamine-penicillin *streptomycin*. The cells were maintained at
30
31 37°C in a humidified atmosphere of 5% CO_2 . Cells after reaching 80-90% confluence were
32
33 trypsinized and seeded on glass coverslips placed in 12-well plate and allowed to adhere for
34
35 overnight. At the time of experiment, complete media was replaced with serum free medium.
36
37 The cells were incubated with receptor **1** (0.9 μM) for 2 hours. After 2 hours of incubation
38
39 with receptor **1**, the cells were then incubated with Zn^{2+} (2.5, 5.0, 10.0 and 25 μM) and HSO_4^-
40
41 (25 μM) for further 1 hour. The cells were washed twice with Phosphate Buffer Saline (1X
42
43 PBS) and then fixed with 100% methanol for 5 minutes and further washed with 1X PBS for
44
45 10 minutes. The cover slip was then mounted on a glass slide using glycerol and observed
46
47 under fluorescence microscope (Leica DMI 6000B) using 20X objective under UV filter. The
48
49 fluorescence images of cells were captured through an attached CCD camera using LAS
50
51 software.
52
53
54
55

56 **3. Results and discussion**

3.1. Synthesis and characterization

A mixture of 2-aminopyridine-3-carbaldehyde and isonicotinohydrazide in 1:1 molar ratio was subjected to undergo condensation under refluxed condition in ethanol to get the required Chemosensor **1**, (E)-N'-((2-hydroxypyridine-3-yl)methylene)isonicotinohydrazide (**Scheme 1**). The Chemosensor **1** was characterized by elemental (C, H, and N) analyses and various spectroscopic ($^1\text{H-NMR}$ and $^{13}\text{C-NMR}$, **Fig. S1-S2**, SI) measurements. Finally, the molecular structure of the Chemosensor **1** was determined by single crystal XRD. An ORTEP diagram of Chemosensor **1** is depicted in **Fig. 1**, and the details of the crystallographic data are summarized in **Table S1 (SI)**. Also, the supplementary crystallographic data for this chemosensor was submitted in the Cambridge Crystallographic Data Centre with CCDC number 982805, and can be obtained free of charge via www.ccdc.cam.ac.uk/data_request/cif.

Chemosensor **1** was crystallized in a tetragonal system with space group I 4(1)/a. Some selected bond lengths and bond angles are given in **Table S2 (SI)**. The crystal structure of Chemosensor **1** exposes that the three donor atoms N (1), N (2) and O (1) are pre-organised in a meridional plan for the encapsulation of metal ion (**Fig. 1**). There is extremely small divergence from planarity in this molecule, an outcome of conjugation between the two aromatic ring systems via the hydrazone connection. The structure of Chemosensor **1** was closely similar to other reported isonicotinoyl derivatives [17]. Even, if the final accepts a less planar conformation with isonicotinoyl ring being twisted by $122.2(1)^\circ$ about the connecting N (1)-C (1)-C (5) bond. In the present structure, the corresponding twist angle is C(6)-N(3)-N(4) is $115.5(1)^\circ$. Intermolecular stacking of electron deficient isonicotinoyl and electron rich 2-aminopyridine-3-carbaldehyde ring at a distance around of a N(3)-C(6) is $1.279(2)^\circ$ is present the structure.

Fig. 1.

3.2. UV-Vis absorbance study

The absorption spectral properties of Chemosensor **1** were studied in 50 % aqueous CH₃CN upon addition of various metal ions such as K⁺, Ca²⁺, Cs⁺, Mg²⁺, Al³⁺, Ba²⁺, Fe²⁺, Fe³⁺, Co²⁺, Ni²⁺, Cu²⁺, Zn²⁺, Hg²⁺, Bi³⁺, Pb²⁺, Cd²⁺, Th⁴⁺, Sr²⁺, Cr³⁺, Mn²⁺ and Ag⁺. Free Chemosensor **1** showed three absorption bands at 256 nm, 286 nm and 358 nm. Upon addition of Zn²⁺, colour of the solution changed from colourless to yellow and discernible changes are observed in the absorption counter of Chemosensor **1**. In the presence of other metal ions (K⁺, Ca²⁺, Cs⁺, Mg²⁺, Al³⁺, Ba²⁺, Fe²⁺, Fe³⁺, Co²⁺, Ni²⁺, Cu²⁺, Hg²⁺, Bi³⁺, Pb²⁺, Cd²⁺, Th⁴⁺, Sr²⁺, Cr³⁺, Mn²⁺ and Ag⁺), Chemosensor **1** showed either no or moderate change in the absorption intensity relative to the free Chemosensor **1** except with Zn²⁺. Also, there were no colour changes attributed to the solution of Chemosensor **1** in the presence of these metal ions. These results suggested a perturbation in the intramolecular charge transfer (ICT) character of the synthesized probe due to the recognition of the Zn²⁺ through imine-N, amide carbonyl and amine groups. This enhances the push-pull character of the ICT state, and consequently a red-shift is observed upon deprotonation and charge transfer between the Chemosensor **1** and Zn²⁺. Further, upon incremental addition of Zn²⁺ (0–2 equiv.) to a solution of Chemosensor **1**, the absorption peak due to the pyridine moiety decreases while a new peak gradually moving to longer wavelength finally reaching a maximum value at 397 nm is observed with the formation of three isosbestic points at 297 nm, 333 nm and 377 nm which indicating the formation of a well-defined **1**-Zn²⁺ scaffold (**Fig. 2**). Under similar conditions, the Chemosensor **1** showed no significant UV-Vis spectral changes in the presence of various anions which inferred that the anions are failed to alter the electronic environment of the chemosensor due to the weak interaction at the ground state [6].

Fig. 2.

1
2
3 The structural optimization of the receptor **1** and its $\mathbf{1}\text{-Zn}^{2+}/\text{HSO}_4^-$ complexes along
4 with the charge transfer process during the encapsulation of analytes (Zn^{2+} and HSO_4^-) by
5 receptor **1** was investigated by density functional theory (DFT) calculations by applying the
6 B3LYP functional, and the basis sets 6-31G** (for C, H, N and O atoms) and LANL2DZ (for
7 Zn atom). All calculations were done by using the computational code Gaussian 09W [22].
8 The optimized structure of receptor **1** was shown in **Fig. 3** and the calculated structural
9 parameters were compared with the X-ray data (**Table S2**). The optimized structure of **1** was
10 superimposed with the X-ray structure which resulted in an acceptable root-mean-square
11 error (RMSE) of 0.243 Å. On complexation of **1** with Zn^{2+} (2:1 ratio) and HSO_4^- (1:1 ratio),
12 the interaction energy ($E_{\text{int}} = E_{\text{complex}} - E_{\text{receptor}} - E_{\text{Zn}^{2+}/\text{HSO}_4^-}$) was lowered respectively by -340.70
13 kcal/mol and -31.66 kcal/mol which clearly delineated the formation of stable complexes
14 (**Fig. 3**). As shown in **Fig. 3**, the receptor **1** preferred to encapsulate Zn^{2+} in a distorted
15 octahedral shape through the amine-N, imine-N and carbonyl-O atoms whereas the HSO_4^-
16 was recognized by multiple intermolecular hydrogen bonds.
17
18
19
20
21
22
23
24
25
26
27
28
29
30
31
32
33

34 Further analysis of frontier molecular orbitals (FMOs) plots of **1** and its $\mathbf{1}\text{-Zn}^{2+}/\text{HSO}_4^-$
35 complexes (**Fig. 4**) indicate that the highest occupied molecular orbital (HOMO) and lowest
36 unoccupied molecular orbital (LUMO) of **1** was resembled with the $\mathbf{1}\text{-HSO}_4^-$ complex and
37 also the band gap was similar. However, an intramolecular charge transfer (ICT) was
38 observed in the $\mathbf{1}\text{-Zn}^{2+}$ complex between the receptor and Zn^{2+} , which resulted in the
39 lowering of band gap in compared to free receptor. Further, the spectral properties were
40 evaluated by TDB3LYP/6-31G** which gave the important absorption for **1**, $\mathbf{1}\text{-Zn}^{2+}$ and $\mathbf{1}\text{-}$
41 HSO_4^- at 378 nm ($f = 0.2917$), 468 nm ($f = 0.004$) and 376 nm ($f = 0.3818$), respectively. The
42 above results accord well with the experimentally determined selectivity of **1** by absorption
43 spectroscopy towards Zn^{2+} and HSO_4^- .
44
45
46
47
48
49
50
51
52
53
54
55
56
57
58
59
60

1
2
3
4
5
6
7
8
9
10
11
12
13
14
15
16
17
18
19
20
21
22
23
24
25
26
27
28
29
30
31
32
33
34
35
36
37
38
39
40
41
42
43
44
45
46
47
48
49
50
51
52
53
54
55
56
57
58
59
60

Fig. 3.

Fig. 4.

3.3. Fluorescence study

In fluorescence study, Chemosensor **1** in 50 % aqueous CH₃CN was investigated for the recognition towards metal ions (K⁺, Na⁺, Mg²⁺, Al³⁺, Cs⁺, Ba²⁺, Ca²⁺, Sr²⁺, Cr³⁺, Mn²⁺, Fe²⁺, Fe³⁺, Co²⁺, Ni²⁺, Cu²⁺, Zn²⁺, Cd²⁺, Bi³⁺, Hg²⁺, Pb²⁺, Ag⁺ in H₂O) and TBA salts of F⁻, Cl⁻, Br⁻, I⁻, AcO⁻, NO₂⁻, NO₃⁻, CN⁻, H₂PO₄⁻, HSO₄⁻ and various oxyanions of sulphur (SO₃⁻, HSO₃⁻ and S₂O₅⁻). As shown in **Fig. 5a** and **5b**, the weakly fluorescent Chemosensor **1** showed highly selective enhancement in the emission wavelength at 470 nm and 425 nm for Zn²⁺ and HSO₄⁻ ion respectively upon excitation at 300 nm. The fluorescence ratio displayed in **Fig. S3a and b (SI)** clearly delineated that after addition of Zn²⁺ and HSO₄⁻ to the solution of Chemosensor **1**, the fluorescence intensity was enhanced selectively. There were no changes in the fluorescence emission of Chemosensor **1** in the presence of other cations and anions tested. The fluorescence of Chemosensor **1** is enhanced upon addition of Zn²⁺ and HSO₄⁻ ions can be attributed to the inhibition of the C=N isomerisation at the excited state [18-19].

Fig. 5.

The fluorescence titrations of Chemosensor **1** were carried out by gradual addition of various concentrations (0–2 equiv.) of Zn²⁺ (**Fig. 6a**) and HSO₄⁻ (**Fig. 6b**). Addition of both the analytes caused a remarkable enhancement in the fluorescence of the chemosensor. In the presence of Zn²⁺, a gradual increase up to 51-fold of the fluorescence was observed at 470 nm upon addition of 2000 μL of Zn²⁺ solution. However, upon addition of HSO₄⁻ to Chemosensor **1** solution, the maximum enhancement of 17-folds was observed at 425 nm due to gradual addition up to 2000 μL. From fluorescence titration data, the detection limit of

1
2
3 Chemosensor **1** as a fluorescent sensor for the analysis of Zn^{2+} and HSO_4^- were found to be
4
5 3.81 nM and 0.95 nM, which is superior than the recently reported Zn^{2+} and HSO_4^- sensors
6
7 (**Table S3**)[23-38], having a dynamic range of 0-200 nM for Zn^{2+} and 0-150 nM for HSO_4^-
8
9 ions.

10
11
12 **Fig. 6.**

13
14 The method of continuous variation (Job's plot) was used to determine the 2:1
15
16 stoichiometry in case **1**. Zn^{2+} while in case of **1**. HSO_4^- shows the 1:1 stoichiometry (**Fig. S4**
17
18 **and S5, SI**) [20]. The association constant K_a of **1** for Zn^{2+} and HSO_4^- coordination were
19
20 calculated for 2:1 stoichiometry (host:guest) on the basis of Benesi-Hildebrand methodology
21
22 and were found to be $2.46 \times 10^5 \text{ M}^{-1}$ and $5.00 \times 10^4 \text{ M}^{-1}$ respectively (**Fig. S6-S7, SI**) [21]. To
23
24 further elucidate the binding interaction of Chemosensor **1** with HSO_4^- , $^1\text{H-NMR}$ titration
25
26 experiments were carried out in $\text{DMSO-}d_6$ (**Fig. S8**). Upon addition of 4 equiv. of the HSO_4^-
27
28 to the Chemosensor **1**, the proton signals of $-\text{NH}_2$ and $-\text{NH}$ at 8.77 ppm and 12.14 ppm were
29
30 disappeared completely. The shift followed by disappearance of the $-\text{NH}_2$ and $-\text{NH}$ protons
31
32 of **1** on interaction with HSO_4^- supports the deprotonation process. Also, the aromatic
33
34 protons were shifted to upfield, which suggests that the negative charges developed from
35
36 deprotonation of **1** by HSO_4^- are delocalized through the whole chemosensor molecule. The
37
38 broadening of the signals on addition of HSO_4^- ions, also justifies the interaction of HSO_4^-
39
40 ions with receptor **1**.

41 42 43 44 **3.4. Analytical applications**

45
46 To check the practical applicability of Chemosensor **1**, the competitive experiments
47
48 were performed. One important criteria for a chemosensor is to give a specific response for
49
50 the selective detection of target analytes (i.e., Zn^{2+} and HSO_4^-) over a wide range of
51
52 potentially competing cations and anions, and to avoid the cross sensitivity. The competition
53
54 experiments were conducted by recording the fluorescence spectra of **1** in the presence of 1.0
55
56
57
58
59
60

1
2
3 equiv. of Zn^{2+} and HSO_4^- mixed with 1 equiv. of other cations and anions mentioned above,
4
5 respectively. No significant variation in the fluorescence was found by comparison with the
6
7 same amounts of Zn^{2+} and HSO_4^- solution in the presence and absence of other cations and
8
9 anions, and the relative error was less than $\pm 5\%$ (**Fig. 7a** and **7b**). These results point out that
10
11 the recognition of Zn^{2+} and HSO_4^- by Chemosensor **1** is not notably interfered by other
12
13 simultaneous cations and anions. Therefore, the Chemosensor **1** exhibits a high selectivity
14
15 and specificity toward Zn^{2+} and HSO_4^- , and opens a new door for the analytical application
16
17 of **1** in real sample analysis.
18
19

20 21 **Fig. 7: A and B**

22
23 In another attempt, encouraged by the fascinating “off-on” emission profile of **1** in the
24
25 presence of Zn^{2+} and HSO_4^- at 415 nm and 470 nm (**Fig. 8**), two chemical inputs Boolean
26
27 type logic gates with INHIBIT and OR logic functions was explained at the molecular level.
28
29 With respect to inputs, the presence and absence of the two chemical inputs Zn^{2+} and HSO_4^-
30
31 was defined as ‘1’ and ‘0’ states, respectively. The fluorescence intensity of receptor **1** at 415
32
33 nm and 470 nm was taken as output for the logic gate with high and low fluorescence signal
34
35 as ‘1’ and ‘0’, respectively. As summarized in **Fig. 8**, in absence of the inputs (Zn^{2+} and
36
37 HSO_4^-), the receptor showed a low fluorescence and the gate was in off-state. On interaction
38
39 with HSO_4^- , the receptor showed a significant fluorescence enhancement (on-state) both at
40
41 415 nm and 470 nm. However, with the input of Zn^{2+} , the gate was remained in switched-off
42
43 and switched-on state at 415 nm and 470 nm, respectively. Further, when the inputs were
44
45 added together, the receptor fluorescence at 415 nm and 470 was found to be in switched-off
46
47 and switch-on conditions, respectively. As summarized in **Fig. 8b**, the above results clearly
48
49 inferred that the fluorescence signals of receptor **1** at 415 nm and 470 nm and with the two
50
51 chemical inputs (Zn^{2+} and HSO_4^-), logic gates of types INHIBIT and OR can be constructed
52
53
54
55
56
57
58
59
60 at the molecular level.

Fig. 8: A and B***In vitro* cell imaging**

To support the biological utility of the synthetic compound receptor **1**, it has been utilized for sensing Zn^{2+} and HSO_4^- in the culture cells. The cell when incubated with receptor **1** only, no fluorescence was observed from the cells. A gradual enhancement of fluorescent intensity was observed when increasing concentration of Zn^{2+} was added in the culture media. However, no fluorescence was observed in the cells incubated with Zn^{2+} (25 μM) only and HSO_4^- (25 μM) only. These results demonstrate the receptor **1** can be used as marker for sensing Zn^{2+} and HSO_4^- ions in living cells (**Fig. 9**).

Fig 9:

In addition to determination of Zn^{2+} and HSO_4^- ions in various complex matrices of cations and anions, it's worth mentioning that presented sensor fulfill the condition of single receptor multi analyte determination without changing its media or solution. Hence, opens a new end for exploration of receptors for multi analyte determination without any interference from each other or from other potential interfering species. The present sensor was also compared with recently reported sensors for Zn^{2+} and HSO_4^- ions; it is quite evident from the comparison (**Table S3**) that presented sensor show a clear advancement in terms of detection limit for both Zn^{2+} and HSO_4^- ions.

4. Conclusion

In conclusion, we have reported for the first time a highly selective and sensitive dual ions 'turn-on' fluorescence sensor for highly selective detection of Zn^{2+} and HSO_4^- in 50 % aqueous CH_3CN . The proposed fluorescence sensor has lower sensing limit towards Zn^{2+} (3.81 nM) and HSO_4^- (0.95 nM). This highly sensitive, selective, easy and cost-effective fluorometric method will provide immense attention for regular analysis of Zn^{2+} and HSO_4^- . The interesting regarding our synthesis is that no quenching was observed for the addition of

1
2
3 both the analytes after stoichiometric equilibrium. Furthermore, the fluorescence properties of
4
5 **1** were successfully explained by a two chemical inputs (Zn^{2+} and HSO_4^-) OR and INHIBIT
6
7 types logic gate at molecular level. Confocal microscopy experiments show that receptor **1**
8
9 can be used for noticing changes in Zn^{2+} and HSO_4^- levels within living HeLa cells. Future
10
11 arrangements will hub on improving the optical brightness and binding sympathy of this
12
13 third-generation sensor as well as applying receptor **1** and related chemical instruments to
14
15 sensor the cell biology of Zn^{2+} and HSO_4^- .
16
17

18 **Acknowledgement**

19
20 ASK gratefully acknowledge financial support from the Department of Science and
21
22 Technology (DST under Fast Track Scheme-SR/FT/CS-160/2011), Government of India,
23
24 New Delhi and University Grant Commission under SAP-DSA Phase I, New Delhi.
25
26
27
28
29
30
31
32
33
34
35
36
37
38
39
40
41
42
43
44
45
46
47
48
49
50
51
52
53
54
55
56
57
58
59
60

References

1. Lehn J. M, *Supramolecular Chemistry*, VCH, Weinheim, 1995.
2. Sahoo S. K, Sharma D, Bera R. K, Crisponi G, Callan J. F, *Chem. Soc. Rev*; 2012; 41:7195-7227.
3. Beer P D, Gale P A, *Angew. Chem.* 2001; 113:502-532.
4. Bianchi A, Bowman-James K, García-Espan E., Wiley-VCH, New-York, 1997.
5. Katayev E A, Ustynyuk Y A and Sessler J L, *Coord. Chem. Rev.* 2006; 250:3004-3037
6. Tayade K , Sahoo S K, Patil R , Attarde S, Singh N, Kuwar A, *Spectrochim. Acta A. Spectrochimica Acta Part A: Molecular and Biomolecular Spectroscopy.* 2014; 126:312–316.
7. De Silva A P., Fox D B, Huxley H J M, Moody T S, *Coord. Chem. Rev*, 2000; 205:41-57.
8. Jiang P and Guo Z, *Coord. Chem. Rev.*, 2004; 248:205-229.
9. Auld D S, *BioMetals*, 2001; 14:271-313.
10. Cox H, McClendon G L, *Curr. Opin. Chem. Biol.*, 2000; 4:162-165.
11. Fegade U, Sahoo S. K, Singh A, Mahulikar P, Attarde S, Singh N, Kuwar A, *RSC Adv*, 2014; 4:15288-15292.
12. Moyer B A, Delmau L H, Fowler C J, Ruas A, Bostick D A, Sessler J L, Katayev E, Pantos G D, Llinares J M, Hossain M A, Kang S O and Bowman-James K. in *Advances in Inorganic Chemistry*, ed. R.V. Eldik and K. Bowman-James, Academic Press, New York, 2006; 175.
13. Sharma D, Sahoo S K, Chaudhary S, Bera R K, Callan J F, *Analyst*, 2013; 138:3646-3650.
14. Kaur P, Kaur H and Singh K, *Analyst*; 2013, 138:425-428.
15. Zhou Y, Kim H N, Yoon J, *Bioorg. Med. Chem. Lett*; 2010, 20:125-128.

16. Sheldrick G M, SHELXL-97. Program Crystal Structure Refinement. University of Göttingen, Germany, 1997.
17. Richardson D R, Bernhardt P V, JBIC, 1999; 4:266-273.
18. Woodroffe C C, Lippard S J, J. Am. Chem. Soc., 2003; 125:11458-11459.
19. Ngo H T, Liu X, Jolliffe K A, Chem. Soc. Rev, 2012; 41:4928-4965.
20. Job P, Ann. Chim., 1928; 9: 113-203.
21. Benesi H. A, Hildebrand J.H, J. Am. Chem. Soc., 1949;71:2703-2707.
22. Frisch, M.J. et. al., Gaussian 09, G09W®, Gaussian Inc., Wallingford, USA, 2009.
23. Mallick, A., Katayama, T., Ishibasi, Y., Yasuda, M., Miyasaka, H. Analyst, 2011;136: 275-279.
24. Yang, S., Liao, D., Chen, S., Hu, C., Wu, A., Analyst, 2012;137:1553-1555.
25. Fegade, U., Sahoo, S. K., Singh, A., Mahulikar, P., Attarde, S., Singh, N., Kuwar, A., RSC Adv., 2014; 4: 15288-15292.
26. Kaur, R., Singh, J., Saini, A., Singh, N., Kaur, N., RSC Adv., 2014; 4: 48004-48011.
27. Chopra, S., Singh, J., Singh, N., Kaur, N., Anal. Methods, 2014; 6: 9030-9036.
28. Singh, J., Yadav, M., Singh, A., Singh, N., Dalton Trans., 2015; 44: 12589-12597.
29. Río, V., Larrechi, M. S., Callao, M. P., Anal. Chim. Acta, 2010; 676: 28–33.
30. Melchert, W. R., Rocha, F. R.P., Anal. Chim. Acta, 2008; 616: 56–62.
31. Othman, A.M., El-Shahawi, M.S., Abdel-Azeem, M., Anal. Chim. Acta, 2006; 555: 322–328.
32. Lv, Y., Cao, M., Li, J., Wang, J., Sensors, 2013;13: 3131-3141.
33. Gupta, V.K., Al Khayat, M., Minoch, A.K., Kumar, P., Anal. Chim. Acta, 2005; 532: 153–158.
34. Cassella, R. J., Brum, D. M., Lima, C. F., Caldas, L. F. S., de Paula, C. E. R., Anal. Chim. Acta, 2011; 690: 79–85.

- 1
- 2
- 3 35. Li, K., Wang, X., Tong, A., *Anal. Chim. Acta*, 2013; 776: 69–73.
- 4
- 5 36. Wenig, Y., Chen, Z., Wang, F., Xue, L., Jiang, H., *Anal. Chim. Acta*, 2009; 647: 215–
- 6 218.
- 7
- 8
- 9 37. Su, C., Hsia, S., Sun, Y., *Anal. Chim. Acta*, 2014;838: 58–63.
- 10
- 11 38. Jakubaa, R. W., Moffett, J. W., Saito, M. A., *Anal. Chim. Acta*, 2008; 614: 143–152.
- 12
- 13 39. Guinovart, T., Blondeau, P., Andrade, F. A., *Chem Comm.*, 2015, 51, 10377-10380.
- 14
- 15
- 16
- 17
- 18
- 19
- 20
- 21
- 22
- 23
- 24
- 25
- 26
- 27
- 28
- 29
- 30
- 31
- 32
- 33
- 34
- 35
- 36
- 37
- 38
- 39
- 40
- 41
- 42
- 43
- 44
- 45
- 46
- 47
- 48
- 49
- 50
- 51
- 52
- 53
- 54
- 55
- 56
- 57
- 58
- 59
- 60

Figure Captions

Scheme 1. Synthesis of Chemosensor **1**.

Fig. 1. ORTEP drawing of the Chemosensor **1**. Displacement ellipsoids are drawn at the 50% probability level.

Fig. 2. UV-Vis absorption spectra of **1** with increasing concentrations of Zn^{2+} (0-1 equiv.) ion in 50 % aqueous CH_3CN .

Fig. 3. DFT computed optimized structure of the receptor **1** and its $\text{1-Zn}^{2+}/\text{HSO}_4^-$ complexes in the gas phase.

Fig. 4. DFT computed HOMO and LUMO diagrams of receptor **1** and its $\text{1-Zn}^{2+}/\text{HSO}_4^-$ complexes in the gas phase.

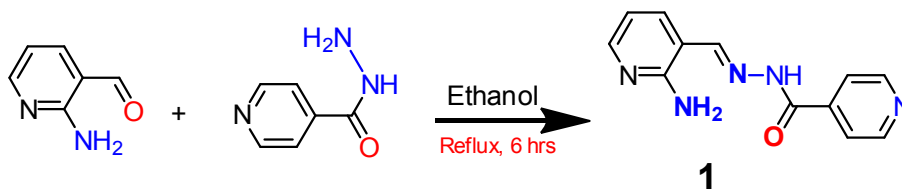
Fig. 5. Selectivity plot of Chemosensor **1** (10 μM) with various (A) cations and (B) anions in 50 % aqueous CH_3CN .

Fig. 6. Titration profile of **1** (10 μM) in 50 % aqueous CH_3CN upon addition of increasing amounts of (A) Zn^{2+} and (B) HSO_4^- ions.

Fig. 7. Competitive fluorescence responses of **1** in the presence of various (A) cations and (B) anions.

Fig. 8. (A) Molecular logic gate behaviour of **1** with the chemical inputs of Zn^{2+} and HSO_4^- by considering the emission changes at 415 nm and 470 nm, and (B) logic scheme and truth table.

Fig 9: The images were taken in an inverted fluorescence microscope (Leica DMI6000B) under 20X objective. A) Phase contrast image of the control cells; B) Fluorescence image of the control cells under UV filter; C) Fluorescence image of the cells treated with receptor **1** only. D) Fluorescence image of the cells treated with receptor **1** for 2 hours and HSO_4^- (25 μM) for 1 hour, E) Phase contrast image of the cells treated with Zn^{2+} (25 μM) only. F) Fluorescence image of the cells treated with receptor **1** for 2 hours and Zn^{2+} (2.5 μM) for 1 hour. G) Fluorescence image of the cells treated with receptor **1** for 2 hours and Zn^{2+} (5 μM) for 1 hour. H) Fluorescence image of the cells treated with receptor **1** for 2 hours and Zn^{2+} (10 μM) for 1 hour. I) Fluorescence image of the cells treated with receptor **1** for 2 hours and Zn^{2+} (25 μM) for 1 hour. J) Fluorescence image of the cells treated with Zn^{2+} (25 μM) only.



Scheme 1.

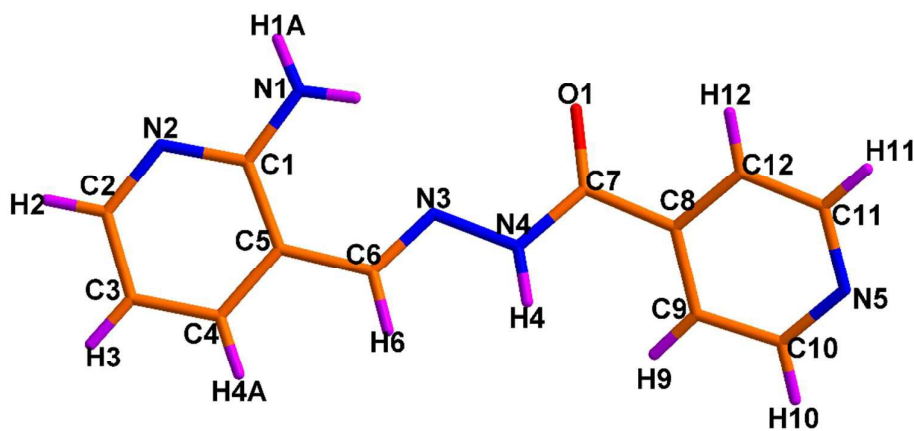


Fig. 1.

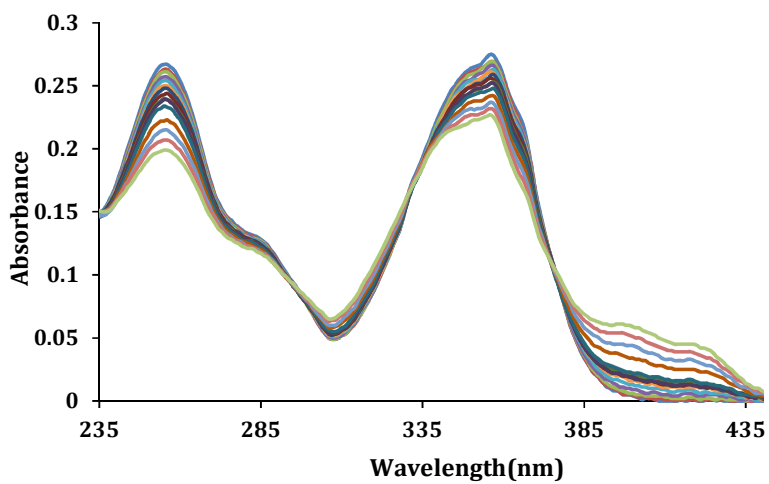


Fig. 2.

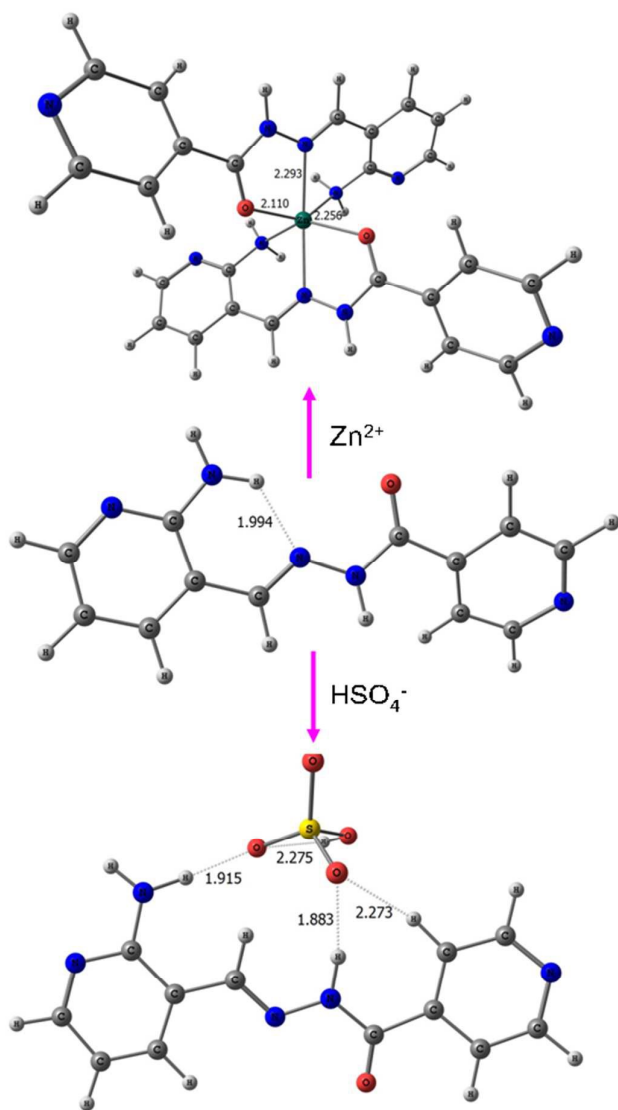


Fig. 3.

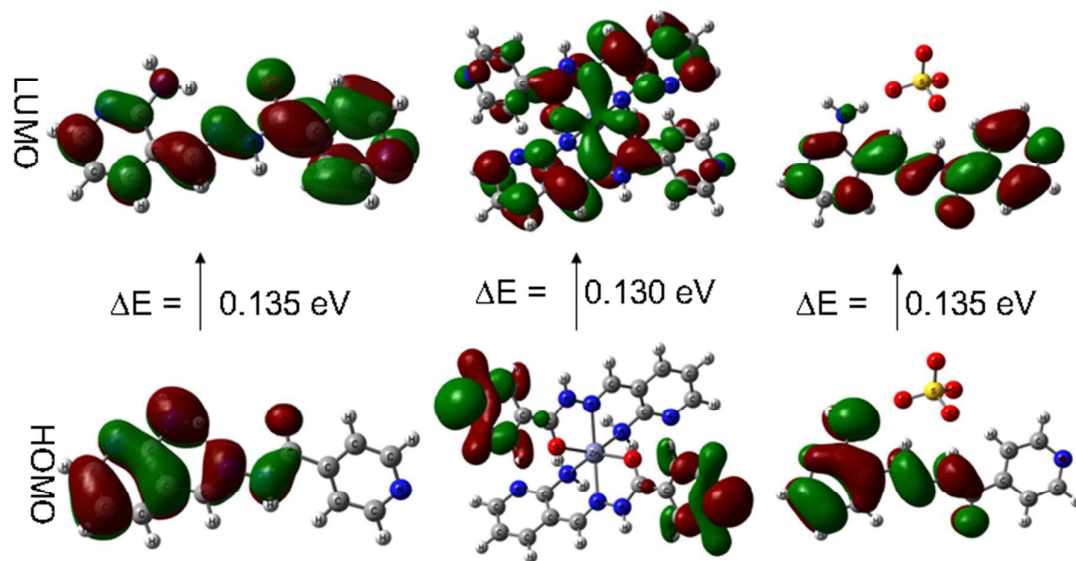
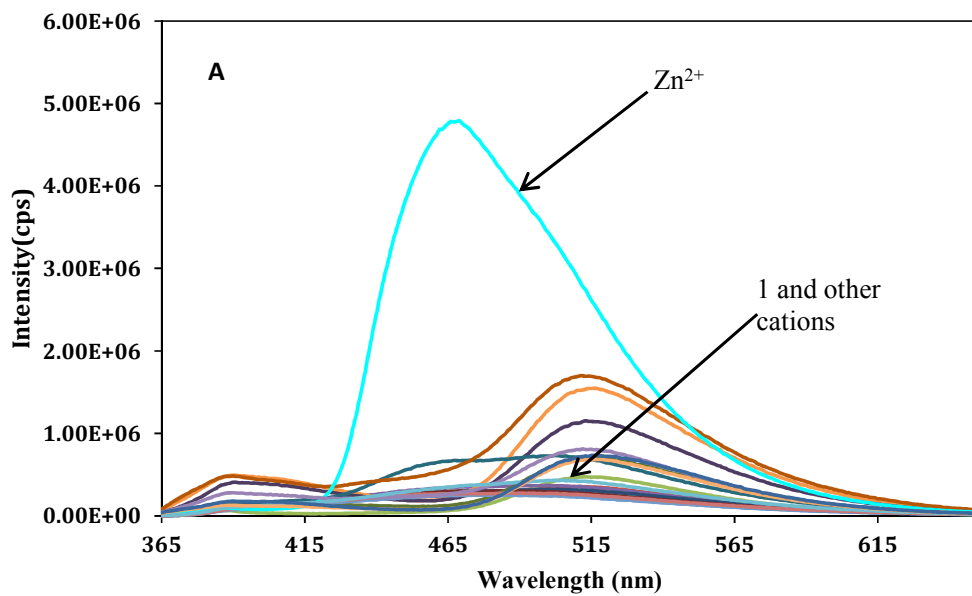


Fig. 4.



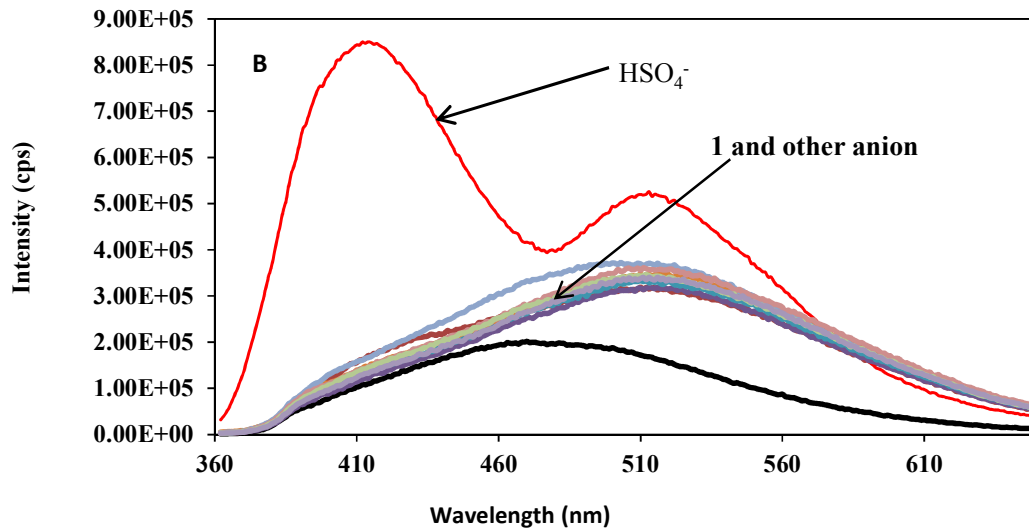
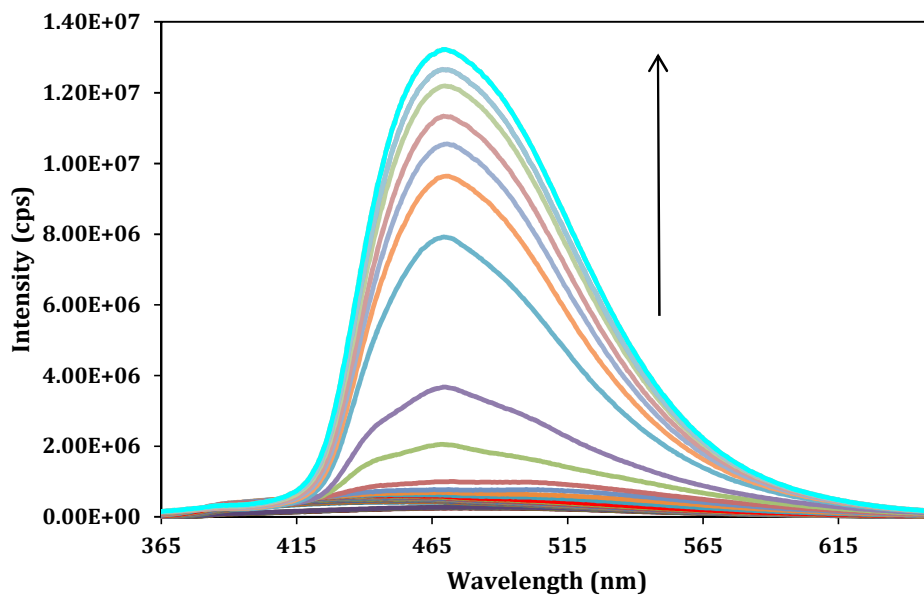


Fig. 5: A and B



Analyst Accepted Manuscript

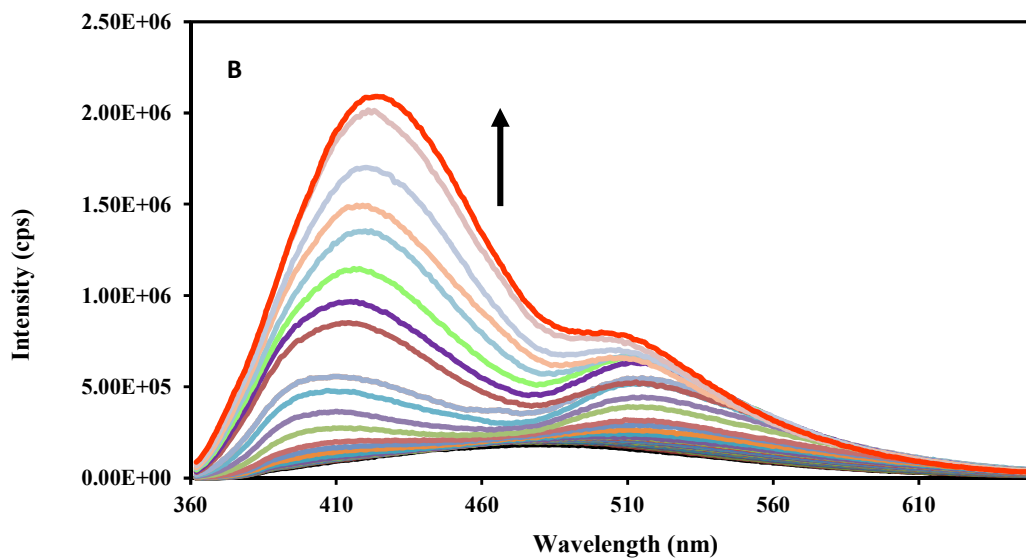
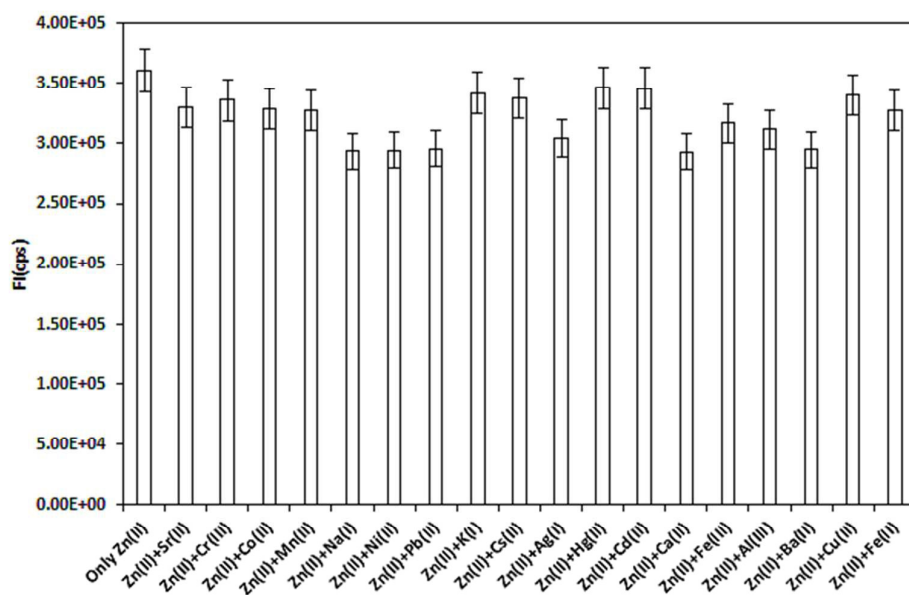


Fig. 6: A and B



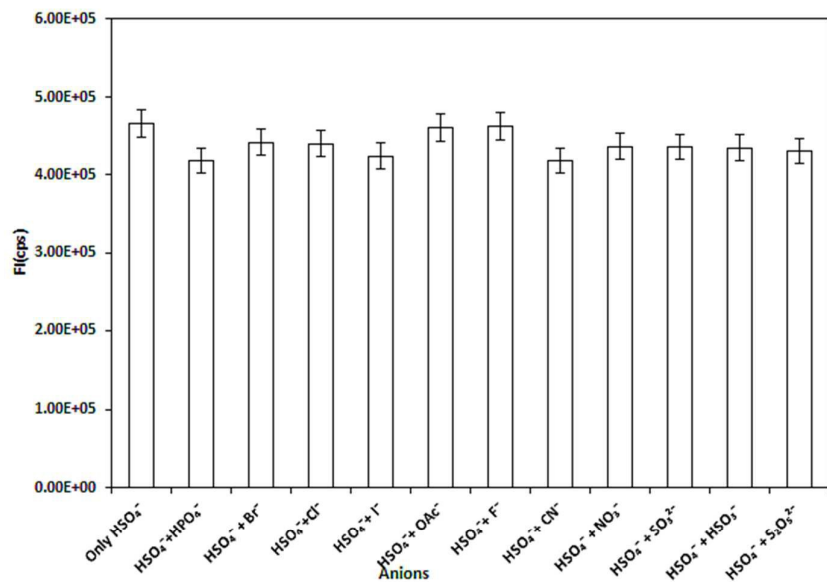


Fig. 7: A and B

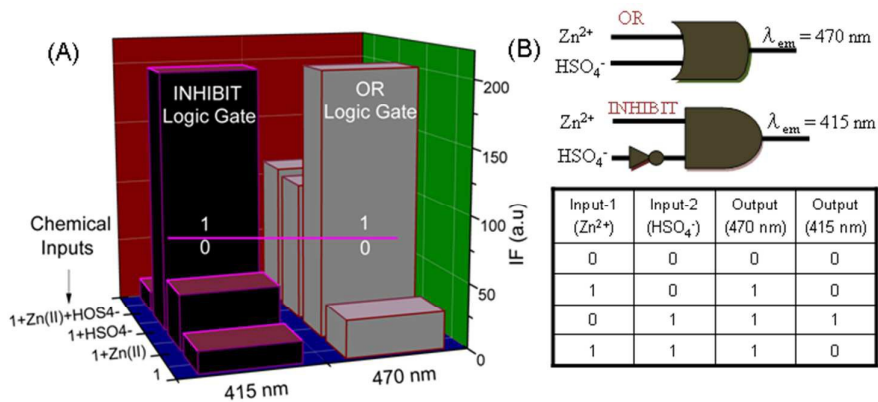


Fig. 8: A and B

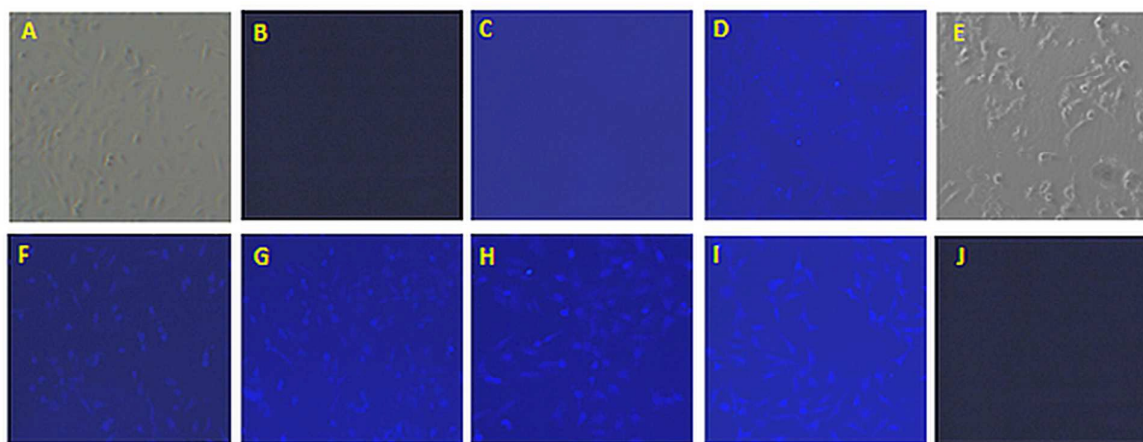


Fig: 9